

Engineered Fullerene-Based Enzyme Mimics for Enhanced Sensing of Aqueous-Phase Reactions Using Liquid Crystals

Deniz Karaman, Elif Akar, Aytül Saylam, Salih Özçubukçu, and Emre Bukusoglu*

Cite This: *ACS Appl. Nano Mater.* 2025, 8, 22798–22808

Read Online

ACCESS |



Metrics & More



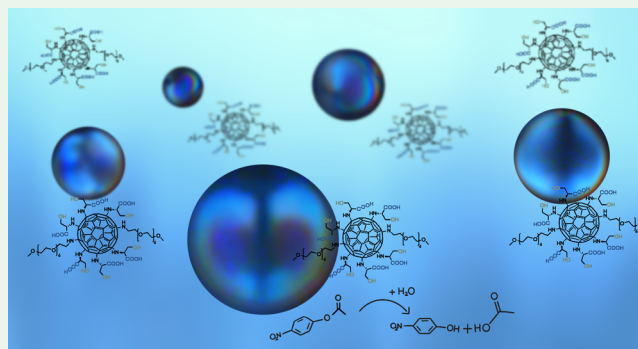
Article Recommendations



Supporting Information

ABSTRACT: The responsive interfaces formed by thermotropic liquid crystals (LC) and aqueous phases have been utilized in reactive and catalytic applications, yet their utilization in enzymatic studies has been dominated by natural enzymes. We introduced fullerene-based enzyme mimics and investigated the enzyme mimic-chemistry-dependent response characteristics of LC–aqueous interfaces. We employed hydrophilic and hydrophobic modifications to the fullerene-based enzyme mimics and performed structure and response characterizations of the LC–aqueous interfaces for tracking aqueous-phase catalytic hydrolysis of *p*-nitrophenyl acetate (*p*NPA) in solutions in contact with nematic 4-pentyl-4'-cyanobiphenyl (5CB) droplets. Polarized light microscopy revealed temporal 5CB droplet configuration changes upon substrate hydrolysis, while interfacial tension measurements and UV–vis spectrophotometry provided insight into adsorption characteristics, interfacial structuration, and reaction kinetics. Our findings demonstrated two distinct interfacial structuring: the enzyme-immobilized interfaces and the interfaces formed with the adsorption–desorption equilibrium of enzyme mimics. We showed that the tailored modifications of fullerene-based enzyme mimics significantly influenced the LC responsiveness toward enzymatic *p*NPA hydrolysis. The design flexibility of fullerene-based enzyme mimics allows for fine-tuned control of interfacial properties, significantly improves LC sensitivity, and promises to advance synthetic enzyme designs for use in biochemical sensing, environmental monitoring, and diagnostic technologies.

KEYWORDS: liquid crystals, emulsions, enzyme mimics, fullerene, hydrolysis, response



1. INTRODUCTION

Thermotropic liquid crystal (LC)–aqueous interfaces are powerful platforms for detecting molecular events through their fluidic and optical properties, which act as “optical amplifiers” for interfacial molecular events.^{1–3} Configured mainly as planar films or LC droplets, these platforms enable versatile chemical and biological detection.^{4,5} Some examples include surfactants, lipids, polymers, DNA, and peptides that induce optically unique LC configurations resulting from their strong interfacial interactions, inducing an alignment change.^{6–11} Studies also report real-time LC ordering changes through enzymatic reactions, including phospholipase A2-catalyzed hydrolysis.^{12–15} A range of other natural enzymes, for example phospholipase C, phospholipase D, lipases, cellulases, α -glucosidases, catalases, and ureases, have been investigated at LC–aqueous interfaces, where their catalytic activities were induced distinct and detectable LC ordering transitions.^{14,16–20} Notably, most of these LC-based sensing studies for monitoring enzymatic activity have employed natural enzymes and rely on analyte adsorption at the LC–aqueous interface to induce LC orientation changes.^{12–14,16,17} This reliance potentially resulted from the difficulty of immobilizing

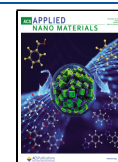
functional natural enzymes at the highly energetic LC–aqueous interface; thus, the enzymatic degradation of these adsorbed molecules can be investigated by adding natural enzymes to the aqueous phase. Recent progress has expanded LC sensing to monitor dynamic catalytic and photocatalytic systems, such as the UV light-driven photo-oxidation of 4-pentyl-4'-cyanobiphenyl (5CB) into 4'-cyano-4-biphenylcarboxylic acid (CBCA) on anatase (101) surfaces, where the photocatalytic transformation induces detectable ordering transitions and thus enables the readout of the catalytic activity.²¹ Recently, we showed that nematic LCs can monitor chemical changes in bulk reactions during the hydrolysis of *para*-nitrophenyl acetate (*p*NPA), catalyzed by synthetic enzyme mimics, which were histidine and serine conjugated fullerene structures (F–HS).²² We demonstrated that the

Received: September 15, 2025

Revised: November 6, 2025

Accepted: November 6, 2025

Published: November 13, 2025



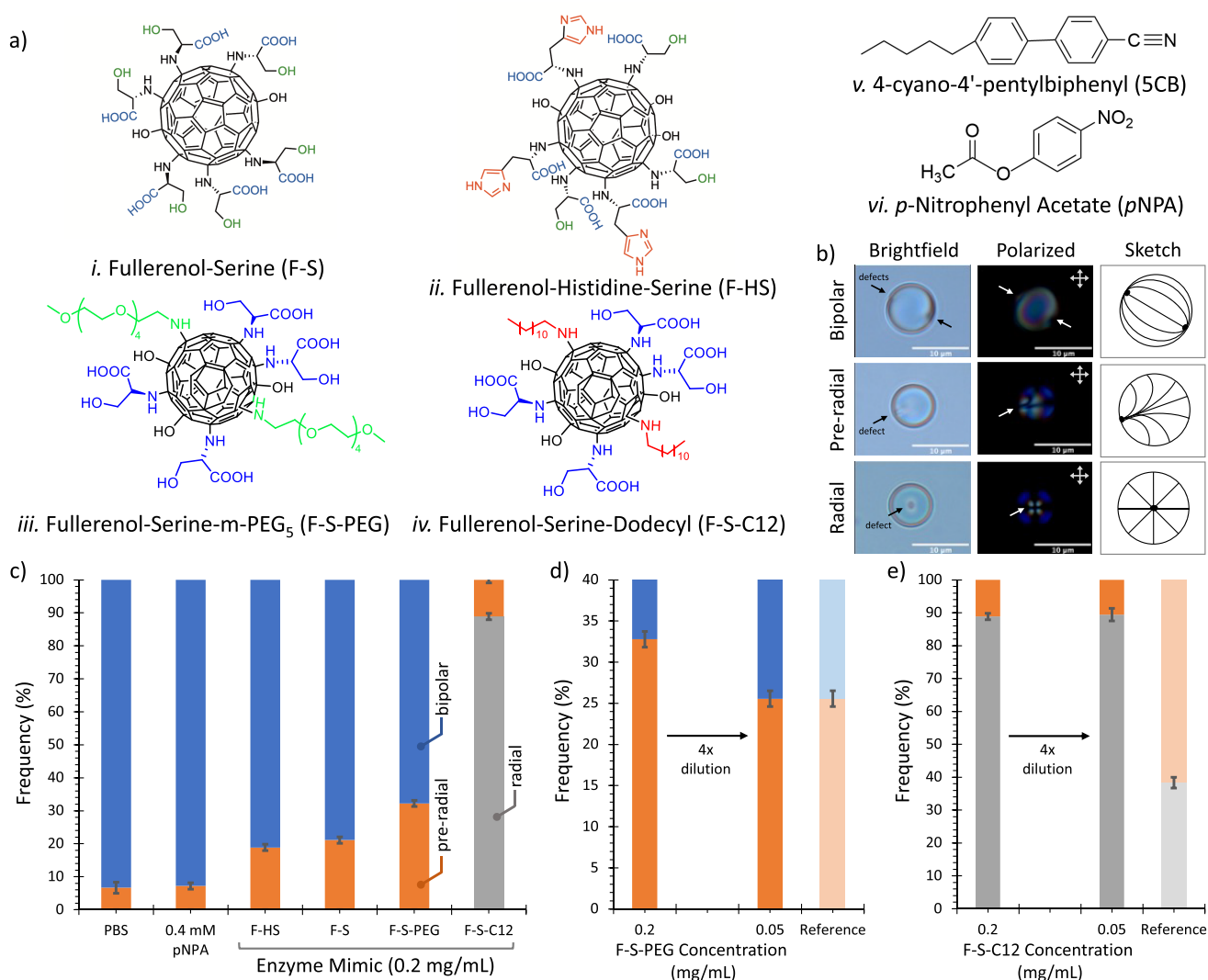


Figure 1. (a) Molecular structures of the enzyme mimics and substrate used in the study: i. fullerene-serine (F-S), ii. fullerene-histidine-serine (F-HS), iii. fullerene-serine-m-PEG₅ (F-S-PEG), iv. fullerene-serine-dodecyl Amine (F-S-C12), v. 4-Cyano-4'-pentylbiphenyl (5CB), vi. *p*-Nitrophenyl acetate (pNPA). (b) Brightfield (left) and polarized light microscopy (middle) images of three 5CB droplets, depicting bipolar, preradial, and radial configurations, as shown in the sketch (right). (c) Configuration distribution of 5CB droplets dispersed in PBS, 0.4 mM pNPA solution, and 0.2 mg/mL solutions of F-HS, F-S, F-S-PEG, and F-S-C12 enzyme mimics ($n = 3$). (d) Configuration distribution of 5CB droplets dispersed in 0.2 mg/mL of F-S-PEG solutions before and after dilution to 0.05 mg/mL with PBS solution ($n = 3$). Reference data reflects the configuration frequency distribution of the 5CB droplets dispersed directly in 0.05 mg/mL F-S-PEG solution ($n = 3$). (e) Configuration distribution of 5CB droplets dispersed in 0.2 mg/mL of F-S-C12 solutions before and after dilution to 0.05 mg/mL with PBS solution ($n = 3$). Reference data reflects the configuration frequency distribution of the 5CB droplets dispersed directly in 0.05 mg/mL F-S-C12 solution ($n = 3$).

nematic LC droplets enable the tracking of the enzymatic activity of the stable, covalently bonded structure of the fullerene-based enzyme mimics, without influencing their bulk kinetics.²² In this work, we sought to extend the capabilities of the fullerene-based enzyme mimic platform by chemical modifications—via PEGylation and alkylation—to control their interactions with the substrates at the LC-aqueous interface. By investigating these chemical modifications, we take an initial step toward developing a versatile and enhanced sensing platform.

Natural enzymes are characterized by complex three-dimensional structural arrangements that demand precise structural motifs to preserve catalytic activity under specific physiological conditions.^{23,24} Conversely, synthetic enzyme

mimics have emerged as versatile alternatives to mimic enzymatic activity by using simplified, minimal systems that depend on carefully designed spatial arrangements and self-assembly processes driven by secondary interactions such as electrostatic forces, hydrogen bonding, and peptide organization.^{25–28} Among these examples, the robust platform of fullerene and fullerene derivatives serves potential for enzyme mimicry purposes through chemical modifications that enable their functionality in photodynamic therapy, electrochemical biosensing, and related biological fields; such modifications include PEGylation, which enhances both solubility and reactivity.^{29–31} Additionally, amine-functionalized C₆₀ fullerene structures demonstrate high catalytic efficiency and robust stability in organic reactions, such as Knoevenagel condensa-

tion.³² The fullerene-based enzyme mimics display significant stability and modularity through their rigid frameworks, which are covalently bonded, thus making them effective for various applications.^{33,34} Their functionalization can be achieved with amino acids like histidine, serine, and glycine, or small molecules that carry key functional groups found in the catalytic site of the target natural enzyme, such as ethanolamine and histamine, or combinations of them to create different hydrolase mimics.³³ Additionally, their structure allows incorporation of functional groups for target recognition, as exemplified by nickel-functionalized serine–histidine fullerenes that exhibit enhanced esterase-like activity and high stability in electrochemical detection of acetylcholine, a biomarker of Alzheimer's disease.³⁵ Beyond esterase-like activity, these enzyme mimics also demonstrate phosphatase-like catalytic properties and the ability to promote osteogenic processes.³⁴ When modified with histidine and hydroxyl-containing amino acids, such as threonine, they can exhibit carbonic anhydrase-like (CA-like) activity.³⁶ In contrast to systems relying on secondary interactions, fullerene-based mimics serve as single-unit catalysts, facilitating straightforward chemical modifications at interfaces. This enables the exploration of molecular interactions using LCs and the elucidation of their responsive character in dynamic aqueous environments.

In this study, we leveraged the sensitivity of LC–aqueous interfaces to chemically modified fullerene-based enzyme mimics to develop a versatile sensing platform for biomolecular interaction detection in aqueous solutions. To regulate their catalytic activity and interfacial interactions, we synthesized serine conjugated-fullerenol (F–S) enzyme mimics containing hydrophilic (by PEGylation, F–S–PEG), hydrophobic (by C12 alkyl chains, F–S–C12) modifications, which also introduce steric effects that influence substrate accessibility. We monitored temporal configuration distributions in nematic LC droplets dispersed in aqueous media, which demonstrated significant sensitivity to the chemical modifications of enzyme mimics using polarized optical microscopy. We established a relationship between molecular structure of the enzyme mimics, their catalytic efficiency, and interfacial structuring, through systematic examination of LC droplet responses in the catalytically active medium. Our study shows that LC droplets provide highly sensitive optical probes that exhibit distinct optical signals to identify subtle modifications to the chemistry of synthetic enzyme systems. This work emphasizes the potential of strategically designed enzyme mimics for improving LC sensor responses by providing a modular and adjustable system. These results suggest that enzyme mimics may be chemically tailored to provide amplified and adaptable LC responses, enabling complex biomolecular sensing applications in environmental monitoring and biochemical research.

2. MATERIALS AND METHODS

2.1. Materials. 4-Cyano-4'-pentylbiphenyl (5CB, a room-temperature nematic LC) was purchased from HCCH Jiangsu Hecheng Chemical Materials Co. Ltd. (Nanjing, China). Dimethyl sulfoxide (DMSO) and phosphate-buffered saline (PBS) tablets (pH of 7.4) were obtained from Sigma-Aldrich (St. Louis). *p*-Nitrophenyl acetate (*p*NPA) was acquired from EMS (Hatfield, PA). *p*-Nitrophenol (*p*NP) was provided by Riedel-de Haën (Seelze, Germany). L-Serine, L-histidine, m-PEG₅-NH₂, and 4-nitrophenyl chloroformate were obtained from BLD Pharmatech Ltd. (Shanghai, China). Tetrabutylammonium hydroxide (TBAH), 4-dimethylaminopyridine (DMAP),

and dodecyl amine were supplied from Acros Organics (Geel, Belgium). Triethylamine was sourced from Sigma-Aldrich (St. Louis, MO, USA). Fullerene C₆₀ (99.5%) was supplied from Nanografi Co, (Ankara, Türkiye). Dichloromethane (DCM) was purchased from Carlo Erba (Milano, Italy). *N,N*-Dimethylformamide (DMF), diethyl ether, isopropanol, methanol, pyridine, toluene, sodium hydroxide, 37% hydrochloric acid, and deuterated solvents were obtained from Merck (Darmstadt, Germany). Sodium hydroxide pellets were purchased from Isolab (Eschau, Germany). Heal Force water purification system (Shanghai, China) was used in the experiments to produce deionized water with a resistance of 18.2 MΩ·cm. Glass slides and coverslips were purchased from Marienfeld GmbH (Lauda-Königshofen, Germany). Interfacial tension measurements were performed using a 3.5 mL quartz cell, and UV–vis experiments were conducted using 96-well plates. KUDOS HP Series 53 kHz high-frequency ultrasonic cleaner was used for sonication. Nuclear magnetic resonance (NMR) spectra of the compounds were recorded on a Bruker Avance DPX 400 MHz spectrometer. FTIR analyses of F–S, F–HS, F–S–C12, and F–S–PEG were performed in a Thermo Scientific Nicolet iS10 FTIR spectrometer in the range of 550–4000 cm⁻¹.

2.2. Synthesis and Characterization of Enzyme Mimics. The molecular structures of the enzyme mimics used in the study are shown in Figure 1a. The synthesis and characterization procedures for the enzyme mimics are explained in details as follows and sketched in Figure S1.

2.2.1. Synthesis of Fullereneol. Fullerene (0.16 g) was dissolved in 100 mL of toluene. To this solution, aqueous NaOH (1.0 g/mL) and 5–6 drops of 30% hydrogen peroxide were added sequentially. 1.0 mL of tetrabutylammonium hydroxide (10% in water) was then added. The reaction mixture was stirred at room temperature for 5 days. After completion, the toluene layer was decanted, and the resulting precipitate was washed with ethanol to remove residual TBAH and other impurities.

2.2.2. Synthesis of Activated Fullereneol. Fullereneol (0.12 g, 0.10 mmol) was dissolved in 15 mL of anhydrous dimethylformamide (DMF) and sonicated for 1 h. To the resulting solution, *p*-nitrophenyl chloroformate (0.80 g), anhydrous pyridine (4.0 mL), and *N,N*-dimethyl aminopyridine (DMAP, 0.040 g) were added at 0 °C. The reaction mixture was stirred under a nitrogen atmosphere for 2 days, with sonication applied twice daily for 1 h. The resulting product was precipitated by the addition of diethyl ether and collected by filtration. The precipitate was washed sequentially with dichloromethane, isopropyl alcohol, and diethyl ether.

2.2.3. Synthesis of Fullereneol–Serine (F–S) and Fullereneol–Histidine–Serine (F–HS). Activated fullereneol (60 mg, 0.030 mmol) was dissolved in 20 mL of anhydrous DMF and sonicated for 1 h. L-serine (0.13 g, 1.2 mmol) was then added to the solution, and the reaction mixture was stirred under N₂ atmosphere for 2 days. Sonication was applied twice daily for 1 h. Upon completion of the reaction, diethyl ether was added to the mixture to precipitate the product. The precipitate was collected by centrifugation, then washed with dichloromethane containing a few drops of methanol followed by diethyl ether. ¹H NMR and FTIR spectroscopy was used for characterization; spectra are shown in Figures S2, S6–S7. Same procedure was applied to synthesize F–HS with 40 mg of activated fullereneol, 20 mL of anhydrous DMF, 42 g of L-serine and 62 g of L-histidine (Figure S3).

2.2.4. Synthesis of Fullereneol–Serine–PEG₅ (F–S–PEG). Activated fullereneol (75 mg, 0.038 mmol) was dissolved in 30 mL of anhydrous DMF and sonicated for 1 h. L-Serine (79 mg, 0.75 mmol) was then added to the solution with the addition of triethyl amine (0.10 mL, 0.75 mmol) and m-PEG₅-NH₂ (0.40 mL, 1.5 mmol). The reaction mixture was stirred under nitrogen atmosphere for 2 days. Sonication was applied twice daily for 1 h. After completion of the reaction, diethyl ether was added to the mixture, and the precipitate was collected by centrifugation. The resulting residue was washed sequentially with dichloromethane containing a few drops of methanol followed by diethyl ether. ¹H NMR and FTIR spectroscopy was used for characterization; spectra are shown in Figures S4, S8–S9.

2.2.5. Synthesis of Fullerene–Serine–Dodecyl Amine (F–S–C12). Activated fullerene (75 mg, 0.038 mmol) was dissolved in 30 mL of anhydrous DMF and sonicated for 1 h. L-Serine (79 mg, 0.75 mmol) and dodecyl amine (0.28 g, 1.5 mmol) were added to the solution. The reaction mixture was stirred under nitrogen atmosphere for 2 days. Sonication was applied twice daily for 1 h. After completion of the reaction, diethyl ether was added to the mixture, and the precipitate was collected by centrifugation. The resulting residue was first washed with dichloromethane containing a few drops of methanol, then diethyl ether. ^1H NMR and FTIR spectroscopy was used for characterization; spectra are shown in Figures S5, S10–S11.

2.3. Preparation of LC Emulsions in Enzyme Mimic Solutions. F–HS (M_w : 2068 g/mol), F–S (M_w : 1690 g/mol), F–S–PEG (M_w : 1550 g/mol), and F–S–C12 (M_w : 2180 g/mol) enzyme mimics were prepared in 1 mL of phosphate-buffered saline (PBS) at varying concentrations (0.05–0.2 mg/mL). F–HS, F–S, and F–S–PEG samples were vortexed for 1 min at 3000 rpm, then they were sonicated for 15 min in an ultrasonic bath. On the other hand, F–S–C12 enzyme mimic samples were subjected to 60 min of sonication in an ultrasonic bath and 80 min of tip-sonication, with a 1 min vortexing at 3000 rpm every 20 min. *p*-Nitrophenyl acetate (*p*NPA) and *p*-nitrophenol (*p*NP) stock solutions at 100 mM were prepared in dimethyl sulfoxide (DMSO) and diluted to the desired concentrations for experiments. To prepare emulsions, 1 mL of aqueous phase samples containing enzyme mimics, *p*NPA, *p*NP, fullerene, or their combinations were mixed with 3 μL of SCB. It was then dispersed for 10 s at 3000 rpm using a vortex mixer. For pH adjustment of the enzyme mimic solutions to 2, 4, 10, or 12, stock solutions of hydrochloric acid and sodium hydroxide were prepared in ultrapure water and subsequently introduced into the enzyme mimic solutions. The molecular structures of the substrate *p*NPA and SCB used in this study are shown in Figure 1a.

2.4. Optical Characterizations of Emulsions. Optical characterizations of LC (SCB) droplet configurations were carried out using a polarized optical microscope (Olympus BX53, Tokyo, Japan) equipped with crossed linear polarizers and a 50 \times long working distance objective lens. 100 μL of each sample was used for the droplet analysis, and at least 60 droplets were examined for each data point. The average results and standard deviations were obtained based on at least three independent experiments. The number of independent experiments (*n*) for each data set is stated along with the experimental results, and the results are shown as the mean \pm standard deviation.

2.5. Interfacial Tension Measurements. The DataPhysics OCA 200 contact angle system (DataPhysics Instruments, Filderstadt, Germany) was used for interfacial tension measurements. For the measurements, 30 μL droplets of SCB were used with a 3.5 mL quartz cell. First, the quartz cell was filled with 2 mL of phosphate-buffered saline (PBS) solution and left to equilibrate for 30 min, with data collection at 15 min intervals. Enzyme mimic solutions were prepared and treated by vortexing, ultrasonication, and tip sonication as appropriate to enzyme type, then added to PBS to reach a concentration of 0.1–0.2 mg/mL. After the addition of the enzyme mimic and mixing in the cuvette, interfacial tension data were taken immediately at 15 min intervals over 150 min to ensure the steady state. For dilution experiments, enzyme mimics were prepared as described above, stabilized for 150 min, and then diluted with fresh PBS to the desired concentrations. Measurement started instantly, and data were collected for an hour at 10 min intervals. Ten consecutive measurements were taken at each time point, and data were derived using the averaged measurements. The mean \pm standard deviation is used to present the results of all experiments, which were conducted in at least three separate repetitions.

2.6. Kinetic Measurement Studies. For enzyme mimic kinetics investigation, an Agilent BioTek Epoch 2 Microplate Spectrophotometer with Gen6 software and 96-well plates were utilized. F–HS, F–S, and F–S–PEG (0.2 mg/mL) samples in PBS were prepared by 1 min vortexing at 3000 rpm, followed by 15 min sonication in an ultrasonic bath, and 15 min of tip sonication. F–S–C12 (0.2 mg/mL) samples were subjected to three steps of processing, which consisted

of 60 min sonication in an ultrasonic bath and subsequent 80 min tip sonication, as well as vortexing at 3000 rpm for 1 min every 20 min. The *p*NPA stock solution of 100 mM concentration was diluted to prepare solutions of 0.4 mM and 1.5 mM, which were added to enzyme mimic solutions. The enzyme mimic solutions were prepared with and without the presence of SCB droplets. The SCB emulsions were prepared in PBS by vortex mixing at 3000 rpm for 1 min, followed by 15 min of ultrasonic bath sonication and tip sonication for 15 min. Absorbance measurements at 410 nm were taken immediately after *p*NPA was added to the enzyme mimics in order to monitor the *p*NP reaction product. The experiments took place at room temperature, while absorbance readings were taken for at least 2 h. The *p*NP concentrations were determined using an extinction coefficient of 11580 $\text{M}^{-1} \text{cm}^{-1}$. The experiments were conducted in three independent runs, and the results are presented as the mean value with standard deviation.

3. RESULTS AND DISCUSSION

We modified the chemistries of fullerene-based enzyme mimics to investigate their interfacial and catalytic activity resulting in changes in the response characteristics of the LC droplets. Our system consists of three essential components dispersed in PBS solutions:

the thermotropic room-temperature nematic LC droplets, 4-pentyl-4'-cyanobiphenyl (5CB),

fullerene-based enzyme mimics, which include the previously reported F–HS,^{22,33,35} and newly used fullerene–serine (F–S), and synthesized fullerene–serine–polyethylene glycol (F–S–PEG) and fullerene–serine–dodecyl amine (F–S–C12) in this study, the substrate *p*-nitrophenyl acetate (*p*NPA).

In F–HS, histidine and serine amino acids were immobilized on the fullerene scaffold, whereas F–S has only serine; F–S–PEG includes polyethylene glycol for increased hydrophilicity and F–S–C12 has dodecyl chains to introduce hydrophobicity in addition to the serine amino acids as shown with representative structures in Figure 1a. These modifications enabled us to probe their influences on ester hydrolysis reactions using the model substrate *p*NPA and the response of 5CB droplets against their interaction with the LC (structured oil)–aqueous interfaces during this hydrolysis activity. The 5CB droplets with sizes within the 1 to 10 μm diameter range were dispersed in enzyme mimic solutions prepared in PBS solution. This size range was selected to allow competition between LC interfacial anchoring and elastic energies.^{5,37}

The formation of distinct nematic 5CB droplet configurations through changes in interfacial anchoring enables the detection of molecular interactions at LC–aqueous interfaces. In the experimental results below, we report the response of the LC droplets as the configuration distributions maintained within a population of droplets in the specific medium with three major configurations shown in Figure 1b. The bipolar configuration exhibits tangential LC orientation with two distinct point defects (boojums) located at opposite poles that produce a dark appearance under crossed polarizers while the surrounding LC regions display bright birefringent colors. The preradial configuration results from tilted interfacial LC alignment, which creates a single point defect at the droplet interface, resulting in a specific optical appearance. The radial configuration involves LC directors aligned normal to the interface, with a central point defect producing a symmetrical four-petal optical appearance under polarized light. We note that these droplet configurations were previously characterized

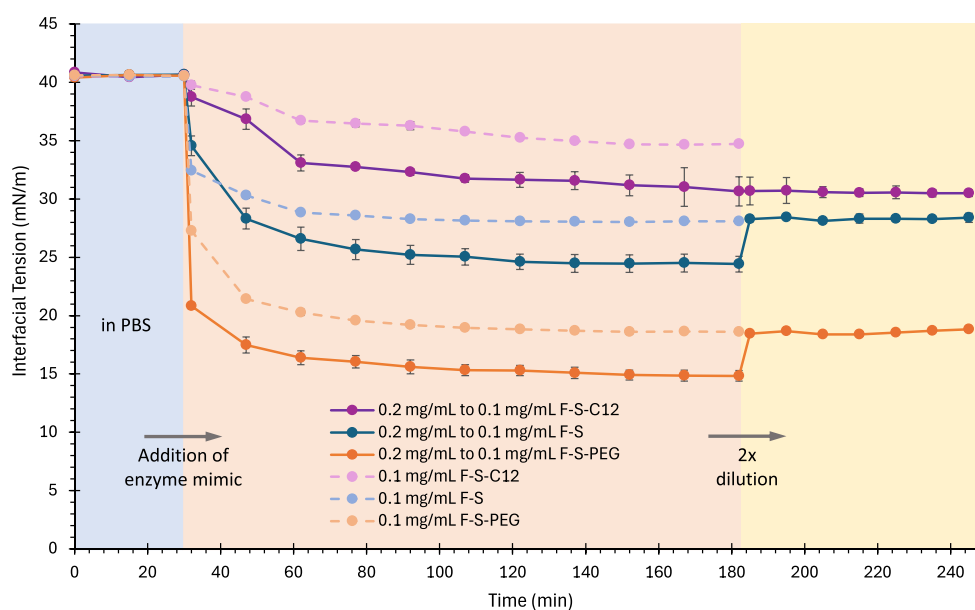


Figure 2. Time-dependent interfacial tension measurements of 5CB-aqueous interfaces equilibrated with solutions of fullerene-based enzyme mimics, F-S-C12, F-S, and F-S-PEG using the pendant drop technique. The data shown as solid lines were obtained at initial enzyme mimic concentrations of 0.2 mg/mL in PBS, followed by their dilution to 0.1 mg/mL using fresh PBS after 150 min of incubation. The data shown with dashed lines were obtained at enzyme mimic concentrations of 0.1 mg/mL in PBS. The data were collected every 15 min before and every 10 min after dilution. Experiments were performed in three independent measurements, reported as mean \pm standard deviation.

for multiple different systems, and the details of the configurations and their energetics can be found elsewhere.^{2,5}

We showed that the baseline configuration distribution of the 5CB droplets dispersed in PBS solutions were $6.7\% \pm 1.7\%$ preradial ($n = 3$) and the rest was bipolar, which was in line with previous reports (Figure 1c).²² Droplets dispersed in solutions of 1 mg/mL fullereneol (no conjugated amino acids) resulted in statistically equivalent results ($7.2\% \pm 1.0\%$ preradial, $n = 3$), indicating its insignificant effect on 5CB droplet configurations as shown in Figure S12. 5CB droplets dispersed in 1 mg/mL solutions of F-HS and F-S enzyme mimics resulted in their configuration distributions that depend on their amino acid content, as shown by the strong dependency of the maintained droplet configuration distributions on the chemical structures of the enzyme mimics (Figure S12). Figure 1c shows the configuration distributions of 5CB droplets induced by the four enzyme mimics (F-HS, F-S, F-S-PEG, and F-S-C12) at 0.2 mg/mL concentrations. We note that these values were time invariant and assumed soon after dispersing the droplets in solutions. As shown, F-HS resulted in bipolar and preradial configurations with a preradial frequency of $18.9\% \pm 1\%$ ($n = 3$) while droplets incubated in solutions of F-S and F-S-PEG resulted in preradial frequencies of $21.1\% \pm 1\%$ ($n = 3$), and $32.2\% \pm 1\%$ ($n = 3$), respectively, where the rest were bipolar. As presented in Figure 1c, 5CB droplets dispersed in solutions of 0.4 mM pNPA resulted in $7.2\% \pm 1.0\%$ ($n = 3$) preradial configuration, and the rest was bipolar, which was statistically indistinguishable from that obtained in PBS ($p > 0.5$). We also measured the interfacial tension of 5CB-aqueous interfaces equilibrated with 0.2 mg/mL solutions of F-HS, F-S, and F-S-PEG (Figure 2, Figure S13), which showed a significant reduction in the interfacial tensions after addition of the enzyme mimics, supporting their interactions with the 5CB-aqueous interfaces. These results revealed that the F-HS, F-S, and F-S-PEG

caused tilted interfacial anchoring of mesogens at aqueous interfaces.

5CB droplets dispersed in 0.2 mg/mL solution of F-S-C12 yielded $88.9\% \pm 1\%$ radial and $11.1\% \pm 1\%$ preradial configurations ($n = 3$) (Figure 1c). This difference was significant when compared to the equivalent results with F-S, F-HS, or F-S-PEG enzyme mimics that caused preradial and bipolar configurations. The alkyl-tailed surfactants SDS, CTAB and DTAB are known to induce homeotropic interfacial anchoring in 5CB droplets, resulting in radial droplet configurations.^{6,7} Thus, this result was reasoned to be due to the alkyl-tailed structure of the F-S-C12 that promoted homeotropic LC anchoring at the aqueous interface, similar to the simple surfactants.

To provide more insight into the interfacial structures of the chemically modified F-S-PEG and F-S-C12 enzyme mimics at the 5CB-aqueous interface, we conducted reversibility experiments to evaluate the changes in configurations and interfacial tensions. As shown in Figure 1d, the preradial configurations of the droplets dispersed in 0.2 mg/mL of F-S-PEG ($32.8\% \pm 1\%$ ($n = 3$)) were reduced to $25.6\% \pm 1\%$ ($n = 3$) upon 4-fold dilution to 0.05 mg/mL with fresh PBS solution. This value was statistically equivalent ($p > 0.5$) to the direct measurements at 0.05 mg/mL F-S-PEG as presented as the “reference” data shown in Figure 1d. The results demonstrated that F-S-PEG underwent a reversible adsorption to the 5CB-aqueous interfaces. Supporting this observation, the recovery of the interfacial tension of 5CB-aqueous phases following the dilution of the aqueous medium of F-S and F-S-PEG solutions demonstrated the effect of reversibility as shown in Figure 2. Conversely, experiments with 5CB droplets dispersed in 0.2 mg/mL of F-S-C12 ($88.9\% \pm 1\%$ radial, $n = 3$) did not reveal a measurable change of their configuration distribution upon dilution to 0.05 mg/mL ($89.4\% \pm 1.9\%$ radial, $n = 3$, Figure 1e). The values deviated substantially from the direct measurements of droplet

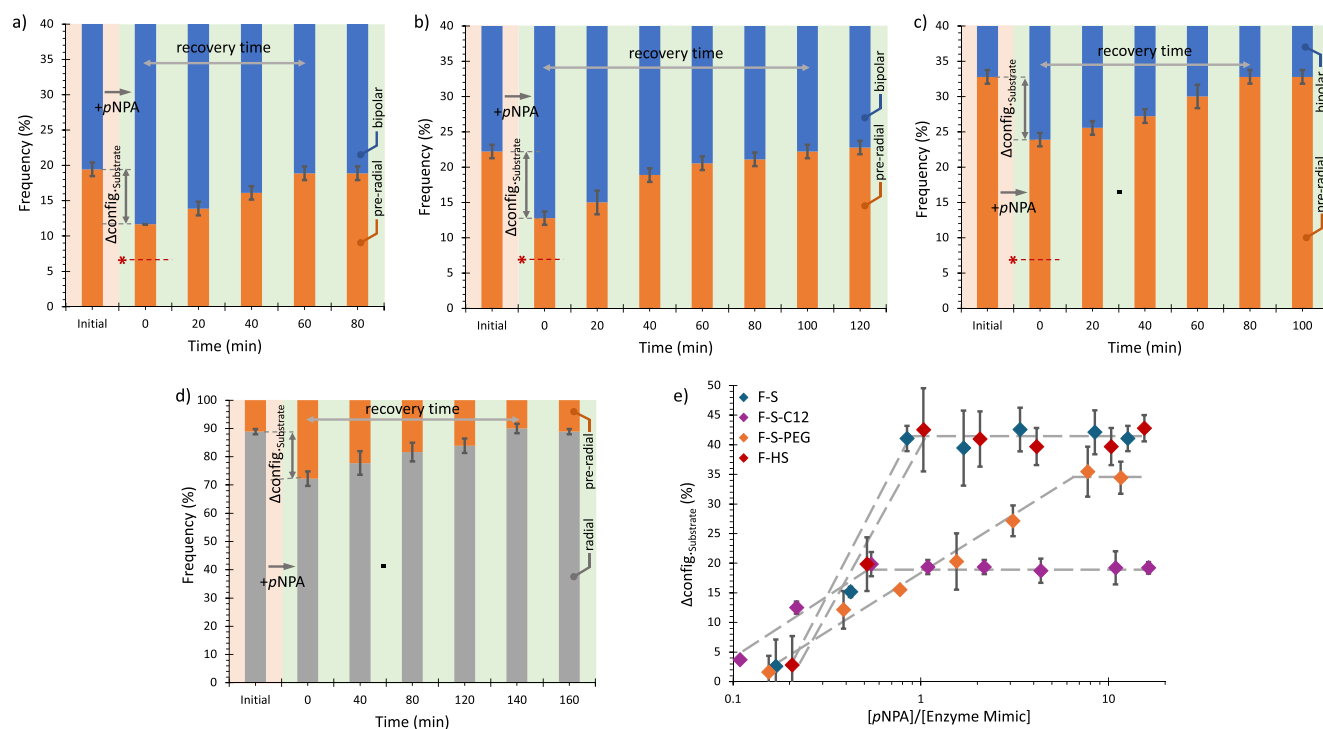


Figure 3. Configuration distributions of 5CB droplets incubated in 0.2 mg/mL solutions of (a) F–HS, (b) F–S, (c) F–S–PEG, (d) F–S–C12, and time-dependent changes in configuration distributions after adding 0.4 mM *p*NPA ($n = 3$). The single-asterisk (*) in (a–c) denotes the preradial configuration frequency induced solely by the *p*NPA solution. (e) Normalized $\Delta\text{config}_{\text{Substrate}}$ as a function of molar ratios of *p*NPA to enzyme mimic ($[\text{pNPA}]/[\text{Enzyme Mimic}]$) for F–HS, F–S, F–S–PEG, and F–S–C12, with enzyme mimic concentrations kept constant at 0.2 mg/mL. $\Delta\text{config}_{\text{Substrate}}$ data are normalized to the configuration frequencies induced by each enzyme mimic. For F–HS, F–S, and F–S–PEG, $\Delta\text{config}_{\text{Substrate}}$ represents the normalized change in preradial configuration frequency induced by *p*NPA in the presence of the enzyme mimic, while for F–S–C12, it represents the normalized change in radial configuration frequency induced by *p*NPA in the presence of the enzyme mimic. Data represent averages and standard deviations from three independent measurements ($n = 3$).

configurations in 0.05 mg/mL F–S–C12 solution as shown in the “reference” data in Figure 1e ($n = 3$). In addition, we did not observe a change in the interfacial tension of 5CB–aqueous interface upon dilution of F–S–C12 solutions from 0.2 mg/mL to 0.1 mg/mL, collectively suggesting their irreversible adsorption to the 5CB–aqueous interface (Figure 2). We reasoned that the alkyl tail terminated structure of F–S–C12 enzyme mimic promoted the hydrophobic interactions between the LC medium and the enzyme mimics to result in the irreversible accumulation of the enzyme mimics at the LC–aqueous interfaces. We demonstrated that chemical modifications to the enzyme mimics bring considerable impact on their adsorption mechanisms, highlighting the crucial function of alkyl chain hydrophobicity in adjusting adsorption characteristics at the 5CB–aqueous interface. Such effects revealed two distinct systems: the first is an interface facilitating a reversible adsorption of enzyme mimics (for F–HS, F–S, or F–S–PEG), whereas the second is an enzyme mimic-immobilized interface (for F–S–C12).

After the characterization of the 5CB droplet responses and the interfacial structures in solutions of enzyme mimics, we investigated the time-dependent configuration distributions of 5CB droplets equilibrated with 0.2 mg/mL solutions of F–HS, F–S, F–S–PEG, and F–S–C12 enzyme mimics upon the addition of *p*NPA substrate. The results for droplets in 0.2 mg/mL F–HS after the addition of 0.4 mM *p*NPA are presented in Figure 3a, and data were collected at 20 min intervals for 80 min. The “initial” data for the 5CB droplet configuration

distributions in the presence of the enzyme mimic in PBS solution alone showed a preradial configuration of $19.4\% \pm 1\%$ ($n = 3$). The initial data, “ $t = 0$ ”, which is the 5CB droplet configurations at the time of *p*NPA addition, exhibited a reduction in preradial configuration frequency to $11.7\% \pm 0\%$ ($n = 3$). The preradial configuration frequency generated by *p*NPA alone, marked with an asterisk (*) in Figure 3a, was found to be $7.2\% \pm 1.0\%$. We note that the reduction at $t = 0$ did not completely reach this value; however, it exhibited a definite trend toward the *p*NPA-only induced configuration distribution, reflecting interactions between F–HS and *p*NPA at the interface. The recovery time, defined as the duration required for the configuration distribution to return to its initial state, was found to be 60 min for the medium of 0.2 mg/mL F–HS and 0.4 mM *p*NPA. The temporal configuration distributions of droplets incubated in 0.2 mg/mL F–S after the addition of 0.4 mM *p*NPA are presented in Figure 3b. The droplet configuration distributions in the presence of the F–S enzyme mimic alone showed a preradial configuration frequency of $22.2\% \pm 1.0\%$ ($n = 3$), which was reduced to a preradial configuration frequency of $12.8\% \pm 1.0\%$ ($n = 3$) after the addition of *p*NPA. In this case, the recovery time was found to be 100 min. The droplet configuration distributions collected at each time point, along with representative micrographs of the droplets at the corresponding time points, are presented in Figure S14. Figure 3c presents droplet configuration distributions over time for droplets incubated in 0.2 mg/mL F–S–PEG solutions after the addition of 0.4 mM *p*NPA. The initial data of preradial

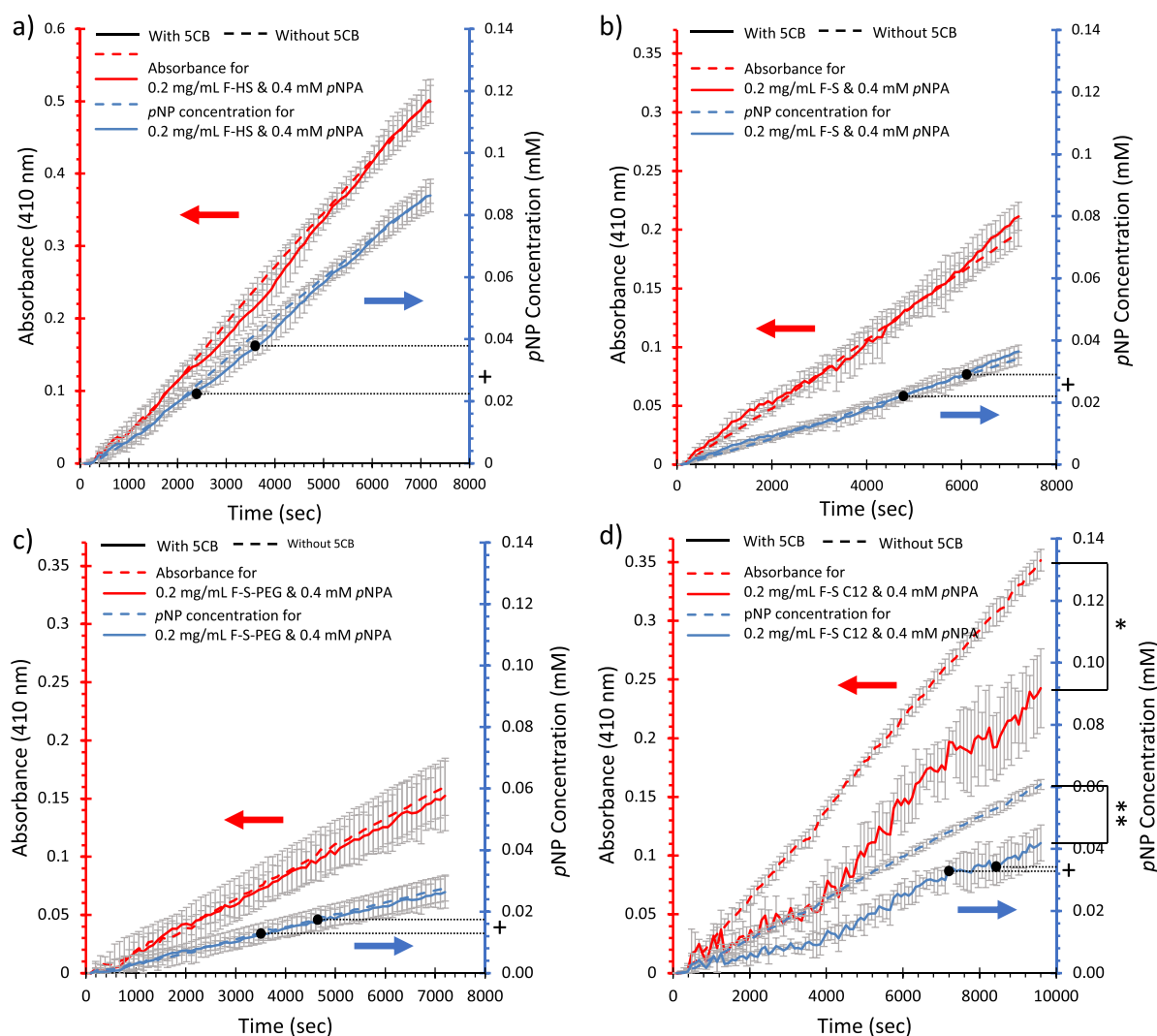


Figure 5. Time-dependent absorbance and corresponding *p*NP concentrations for (a) 0.2 mg/mL F–HS with 0.4 mM *p*NPA (7200 s), (b) 0.2 mg/mL F–S with 0.4 mM *p*NPA (7200 s), (c) 0.2 mg/mL F–S–PEG with 0.4 mM *p*NPA (7200 s), and (d) 0.2 mg/mL F–S–C12 with 0.4 mM *p*NPA (9600 s), measured at 410 nm and room temperature using UV–vis spectroscopy with and without 5CB. Solid lines represent data with 5CB, dashed lines without 5CB. Dark dots (●) represent the recovery time intervals and dotted lines mark *p*NP concentrations at these intervals, with average *p*NP concentration indicated by a plus (+) symbol. Graphs represent mean \pm standard deviation from three independent experiments.

with 0.4 mM *p*NPA as shown in Figure 3a–d, the recovery times at similar $[pNP]/[Enzyme\ Mimic]$ ratios follow the order from shortest to longest: F–HS, F–S–PEG, F–S, and F–S–C12. Experiments on enzyme mimic–*p*NPA interactions indicated that the hydrophilic (F–S–PEG) and hydrophobic (F–S–C12) modifications, in contrast to F–HS and F–S, impart distinct interaction dynamics with *p*NPA, thereby tuning the response of the LCs.

The catalytic activities of 0.2 mg/mL enzyme mimics (F–HS, F–S, F–S–C12, F–S–PEG) at the experimental conditions with (0.3% vol) and without the presence of the dispersed 5CB droplets were determined by measuring *p*NPA hydrolysis. We used UV–vis spectrophotometry to track the formation of *p*NP. Figure 5 is a plot of time-dependent absorbance (left, red axis) and corresponding *p*NP concentrations (right, blue axis) of the 0.4 mM *p*NPA interactions with F–HS (Figure 5a), F–S (Figure 5b), F–S–PEG (Figure 5c), and F–S–C12 (Figure 5d) enzyme mimics. Results from samples containing 5CB are indicated with solid lines, and those without 5CB are indicated with dashed lines. Experi-

ments investigating droplet configurations with 0.2 mg/mL enzyme mimics and 0.4 mM *p*NPA revealed recovery times of 60 min for F–HS, 100 min for F–S, 80 min for F–S–PEG, and 140 min for F–S–C12 (Figure 3). To calculate *p*NP concentrations more accurately, we analyzed recovery times as time ranges: 40–60 min for F–HS, 80–100 min for F–S, 60–80 min for F–S–PEG, and 120–140 min for F–S–C12 (Table 1). The *p*NP concentrations corresponding to these are

Table 1. Recovery Time Intervals of the Droplets Dispersed in 0.2 mg/mL Solutions of Enzyme Mimics and the Average $[pNP]/[pNPA]$ Corresponding to This Time Interval after Addition of *p*NPA

Enzyme Mimic	Recovery Time Interval (min)	$[pNP]/[pNPA]_{ave}$ in 0.4 mM <i>p</i> NPA	$[pNP]/[pNPA]_{ave}$ in 1.5 mM <i>p</i> NPA
F–HS	40–60	0.082 ± 0.023	0.076 ± 0.013
F–S	80–100	0.069 ± 0.011	0.069 ± 0.007
F–S–PEG	80–100	0.039 ± 0.009	0.041 ± 0.006
F–S–C12	120–140	0.092 ± 0.010	0.099 ± 0.016

shown as dark dots (●) on the plots in the presence of 5CB, with the average *p*NP concentration for these ranges indicated with a plus (+) sign. The absorbance and concentrations of *p*NP were linearly incremented within the ranges of recovery times, without showing a noticeable change, which we also explained in more detail in our previous study.²² Thus, the response measured by the configuration changes within the droplets was not due to a change in the kinetic activity of the enzyme mimics.

We investigated the interactions of 0.8 mM *p*NPA—double the amount of *p*NP obtained from the complete hydrolysis of 0.4 mM *p*NPA—with 0.2 mg/mL enzyme mimics (F–HS, F–S, F–S–PEG, F–S–C12) in the absence of *p*NPA. We observed that the addition of *p*NP did not influence the configuration distribution of the 5CB droplets interacting with enzyme mimics (Figure S19). In addition, previous studies have shown that the alignment of LCs at aqueous interfaces is highly sensitive to interfacial charging and pH.^{40,41} To test this possibility, we investigated whether the hydrolysis of *p*NPA could locally alter these conditions at the LC–aqueous interface and thereby contribute to the observed droplet responses. Baseline configuration frequency distributions of 5CB droplets dispersed in pure water containing 0.2 mg/mL F–HS, F–S, F–S–PEG, or F–S–C12 were first obtained, followed by systematic adjustment of the pH to 2, 4, 10, and 12. The configuration frequency distributions of 5CB droplets dispersed in the enzyme mimic solutions were collected immediately after preparation and following 1 h of equilibration. The results revealed that pH variations did not affect the droplet configuration distributions dispersed in any of the enzyme mimics, confirming that the observed transitions were driven by alteration of the interfacial chemistry rather than local variations in pH (Figure S20).

When we quantified the mean $[pNP]/[pNPA]$ ratio within the recovery time interval of the droplets dispersed in F–HS solutions between 40 and 60 min was determined to be 0.082 ± 0.023 using the data shown in Figure 5a (as indicated by the average *p*NP concentration plotted with a plus (+) sign) and as shown in Table 1. For the F–S, the recovery time interval of between 80 and 100 min corresponded to an average $[pNP]/[pNPA]$ of 0.069 ± 0.011 (Figure 5b). For F–S–PEG, as shown in Figure 5c, the recovery time interval between 60 and 80 min yielded an average $[pNP]/[pNPA]$ ratio of 0.039 ± 0.009 . Lastly, for F–S–C12, as shown in Figure 5d, the recovery time interval between 120 and 140 min, marked with dark dots (●), corresponded to an average $[pNP]/[pNPA]$ ratio of 0.092 ± 0.010 . To further investigate the interaction between *p*NPA and the F–S–C12 enzyme mimic, we conducted additional experiments on droplet configuration distributions to examine the catalytic cycling characteristics of the system. After one full recovery cycle of 5CB droplets dispersed in 0.2 mg/mL F–S–C12 and 0.4 mM *p*NPA, a second aliquot of 0.4 mM *p*NPA was introduced into the same dispersion. The configuration frequency distributions of the droplets were monitored for 100 min, and no measurable change in droplet configurations was observed. This result indicated that the droplet response obtained from the interactions between the F–S–C12 enzyme mimic and *p*NPA does not recover after the first catalytic cycle (Figure S21).

In contrast to other enzyme mimics, F–S–C12 forms irreversible enzyme mimic-adsorbed 5CB–aqueous interfaces while demonstrating catalytic activity for the hydrolysis of

*p*NPA. Figure S22 displays the graphs of time-dependent absorbance along with the associated *p*NP concentration for the medium of 0.2 mg/mL of F–HS, F–S, F–S–PEG, or F–S–C12 with 1.5 mM *p*NPA. The $[pNP]/[pNPA]$ ratios averaged over the recovery time ranges of the droplets dispersed in F–HS, F–S, F–S–PEG, and F–S–C12 solutions were 0.076 ± 0.013 , 0.069 ± 0.007 , 0.041 ± 0.006 , and 0.099 ± 0.016 , respectively, which were similar to the ratio using 0.4 mM *p*NPA (Table 1). Correspondingly, based on these two concentrations of *p*NPA, the ratios of $[pNP]/[pNPA]$ at droplet configuration recovery times for the enzyme mimics F–HS, F–S, F–S–PEG, and F–S–C12 of 0.2 mg/mL were 0.079 ± 0.018 , 0.069 ± 0.009 , 0.040 ± 0.007 , and 0.095 ± 0.013 , respectively. The $[pNP]/[pNPA]$ ratio of 0.079 ± 0.018 for 0.2 mg/mL F–HS at the recovery time was lower than the ratio measured as ~ 0.25 with 0.5 mg/mL F–HS in our previous work.²² Such a difference can be reasoned to be the higher partitioning of *p*NP at lower enzyme concentration. Decreased product formation was thus enough for enzyme mimic–substrate–product equilibrium (Figure 5a).

The time-dependent absorbance and *p*NP concentrations measured in solutions of F–HS, F–S, and F–S–PEG enzyme mimics were indistinguishable for the 5CB-containing and 5CB-free samples, showing no measurable influence of the presence of 5CB droplets in the hydrolysis kinetics of the enzymes (Figure 5a–c). To quantitatively compare the catalytic activities of the enzyme mimics, the apparent initial rates of *p*NPA hydrolysis were determined from the linear regions of the UV–vis kinetics curves presented in Figure 5, obtained using 0.2 mg/mL enzyme mimic solutions with 0.4 mM *p*NPA (Table S2). The calculated rates were 12.9 ± 0.7 nM/s in the presence of 5CB and 12.9 ± 0.6 nM/s in its absence for F–HS; 4.9 ± 0.3 nM/s both in the presence and absence of 5CB for F–S; and 3.7 ± 0.7 nM/s with 5CB and 4.0 ± 0.3 nM/s without 5CB for F–S–PEG. These quantitative results indicate that the intrinsic catalytic efficiencies of F–HS, F–S, and F–S–PEG are effectively unchanged by the presence of 5CB droplets.

For the droplets incubated in solutions of F–S–C12, there was a significant reduction of absorbance and the corresponding *p*NP concentrations for 5CB-containing samples compared to 5CB-free samples, as indicated by * and ** in Figure 5d. This result was in line with the experiments reported in Figure 1e, Figure 2, and the discussion on the data related to the irreversible adsorption of the F–S–C12 mimics to the 5CB–aqueous interfaces. When we compared the increase rates of the absorbance and the corresponding *p*NP concentrations measured in cases of F–S, F–S–PEG, and F–S–C12 mimics, F–S–C12 exhibited the highest initial rate of *p*NPA hydrolysis compared to others in the absence of 5CB (6.6 ± 0.2 nM/s, Table S2; Figure 5). However, in the presence of 5CB, the slope of the absorbance and the initial rate of *p*NPA hydrolysis of the case of F–S–C12 decreased significantly to 4.7 ± 0.7 nM/s (Table S2). This value approaches to that measured for F–S–PEG (3.7 ± 0.7 nM/s, Table S2), which possessed the slowest catalytic activity among the enzyme mimics, likely due to the hydrophilic modification and steric hindrance effect (Figure 5c,d). The significant submersion of the F–S–C12 mimics into the 5CB phase due to their hydrophobicity potentially limited the *p*NPA access to the serine-based active sites. The steric hindrance imparted by the C12 tails may also increase this effect by further hindering the partitioning of *p*NPA. In the presence of 5CB–aqueous interfaces, these effects

dramatically lowered the catalytic activity of the F–S–C12 mimics (Figure 5d, Table S2). Furthermore, in contrast to the other enzyme mimics, the $\Delta\text{config-Substrate}$ plateaued at a much lower value for F–S–C12, indicating the limitation of *p*NPA concentration at the enzyme mimic interface (Figure 3e). The prolonged recovery time of the droplet configurations incubated in F–S–C12 solutions compared to the other enzyme mimics further reflects limited *p*NPA access to the active sites and inhibited *p*NP accumulation at the interface due to its hydrophobic character, necessitating higher product conversion to accomplish complete recovery (Figure 4, Table 1). Notably, configurations of the 5CB droplets in F–S–PEG solutions achieved the second-fastest recovery time after F–HS (Figure 3a–d, Figure 4), even though they exhibited the lowest increase rate of the absorbance and the initial rate of *p*NPA hydrolysis among the enzyme mimics (Figure 5, Table S2). This was potentially because the hydrophilic modification in F–S–PEG leads to a low $[pNP]/[pNPA]$ ratio (0.040 ± 0.007), which was sufficient to reach complete recovery. This was possible due to enhanced *p*NP accumulation at the interface, resulting from the hydrophilic nature of PEG chains.

4. CONCLUSION

We presented the tracking of aqueous phase reactions catalyzed by fullerene-based enzyme mimics (F–S, F–HS, F–S–PEG, and F–S–C12) using nematic 5CB droplets dispersed in reaction medium. By investigating the interfacial characteristics and catalytic activity of the enzyme mimics and the dynamic response of the droplets, we examined the influence of hydrophilic (PEG) and hydrophobic (C12) modifications on the hydrolysis of *p*-nitrophenyl acetate (*p*NPA). Unlike other enzyme mimics, F–S–C12 formed “enzyme-immobilized” LC-aqueous interfaces with irreversible adsorption, supported by the interfacial tension measurements and the configuration reversibility measurements. These measurements also revealed that F–S, F–HS and F–S–PEG showed reversible adsorption at the LC–aqueous interfaces. We showed that the chemical modifications significantly influenced the interfacial anchoring of LCs and tuned the enzyme mimic–*p*NPA interactions resulting in significant differences in the LC configuration distributions and recovery times. Such differences were consistent with the hydrophobicity of the modification performed to the enzyme mimic. We demonstrated that such effects improved sensing, with detection at concentrations down to 0.01 mM *p*NPA (for F–S–C12). The addition of *p*NPA to F–S–C12 resulted in stable radial configurations at low *p*NPA concentrations, with extended recovery times, whereas F–S–PEG and F–S demonstrated faster recovery with preradial configuration changes, indicative of different interaction dynamics. Measurements of enzymatic activity studies indicated that the hydrophobic microenvironment of F–S–C12, created by the presence of 5CB and irreversible adsorption, resulted in slower kinetics compared to the medium without 5CB. These modified chemistries of the fullerene-based enzyme mimics highlight the potential of LC interfaces in identifying subtle chemical changes, and the influence of these changes on the intermolecular interactions including the reactions, paving a path for the sensing platforms based on reactive interactions. The specific responses of LC interfaces to chemically engineered enzyme mimics enable their use in diverse applications, including biochemical assays, environmental monitoring, and clinical diagnostics. The study also shows

that two classes of fullerene-based enzyme mimic–LC platforms are possible, one is an “enzyme immobilized interface”, the second is an interface that facilitate a reversible adsorption of enzyme mimics with no influence of LCs on the reaction kinetics. Thus, introducing two systems that the next generation applications can be realized.

■ ASSOCIATED CONTENT

Data Availability Statement

The data that support the findings of this study are available from the corresponding author upon reasonable request.

Supporting Information

The Supporting Information is available free of charge at <https://pubs.acs.org/doi/10.1021/acsanm.5c04258>.

NMR and FTIR results for the synthesized enzyme mimics, additional droplet configuration distribution data, interfacial tension measurements of 5CB interfaces in F–HS solutions, UV–vis absorption measurements (PDF)

■ AUTHOR INFORMATION

Corresponding Author

Emre Bukusoglu – Department of Chemical Engineering, Middle East Technical University, Ankara 06800, Türkiye; Department of Micro and Nanotechnology, Middle East Technical University, Ankara 06800, Türkiye; orcid.org/0000-0002-3128-059X; Email: emrebuk@metu.edu.tr

Authors

Deniz Karaman – Department of Chemical Engineering, Middle East Technical University, Ankara 06800, Türkiye
Elif Akar – Department of Chemistry, Middle East Technical University, Ankara 06800, Türkiye
Aytül Saylam – Department of Chemistry, Middle East Technical University, Ankara 06800, Türkiye; orcid.org/0000-0002-5619-5447
Salih Özçubukçu – Department of Chemistry, Middle East Technical University, Ankara 06800, Türkiye

Complete contact information is available at: <https://pubs.acs.org/10.1021/acsanm.5c04258>

Author Contributions

D.K. conducted experiments and characterizations involving liquid crystals. A.S. and E.A. synthesized and characterized enzyme mimics. D.K., A.S., and E.A. performed measurements of enzyme kinetics. E.B. and S.Ö. supervised the research. All authors contributed to data interpretation, discussions, and manuscript preparation.

Notes

The authors declare no competing financial interest.

■ ACKNOWLEDGMENTS

This work was supported by the Scientific and Technological Research Council of Turkey (TÜBİTAK) under award number 222Z147.

■ REFERENCES

- (1) Gupta, V. K.; Skaife, J. J.; Dubrovsky, T. B.; Abbott, N. L. Optical Amplification of Ligand-Receptor Using Liquid Crystals. *Science* **1998**, *279* (5359), 2077–2080.

- (2) Bukusoglu, E.; Pantoja, M. B.; Mushenheim, P. C.; Wang, X.; Abbott, N. L. Design of Responsive and Active (Soft) Materials Using Liquid Crystals. *Annu. Rev. Chem. Biomol. Eng.* **2016**, *7* (1), 163–196.
- (3) Miller, D. S.; Carlton, R. J.; Mushenheim, P. C.; Abbott, N. L. Introduction to Optical Methods for Characterizing Liquid Crystals at Interfaces. *Langmuir* **2013**, *29* (10), 3154–3169.
- (4) Carlton, R. J.; Hunter, J. T.; Miller, D. S.; Abbasi, R.; Mushenheim, P. C.; Tan, L. N.; Abbott, N. L. Chemical and Biological Sensing Using Liquid Crystals. *Liq. Cryst. Rev.* **2013**, *1* (1), 29–51.
- (5) Miller, D. S.; Wang, X.; Abbott, N. L. Design of Functional Materials Based on Liquid Crystalline Droplets. *Chem. Mater.* **2014**, *26* (1), 496–506.
- (6) Lockwood, N. A.; Gupta, J. K.; Abbott, N. L. Self-Assembly of Amphiphiles, Polymers and Proteins at Interfaces between Thermotropic Liquid Crystals and Aqueous Phases. *Surf. Sci. Rep.* **2008**, *63* (6), 255–293.
- (7) Brake, J. M.; Mezera, A. D.; Abbott, N. L. Effect of Surfactant Structure on the Orientation of Liquid Crystals at Aqueous-Liquid Crystal Interfaces. *Langmuir* **2003**, *19* (16), 6436–6442.
- (8) Gupta, J. K.; Zimmerman, J. S.; De Pablo, J. J.; Caruso, F.; Abbott, N. L. Characterization of Adsorbate-Induced Ordering Transitions of Liquid Crystals within Monodisperse Droplets. *Langmuir* **2009**, *25* (16), 9016–9024.
- (9) Kim, Y. K.; Noh, J.; Nayani, K.; Abbott, N. L. Soft Matter from Liquid Crystals. *Soft Matter* **2019**, *15* (35), 6913–6929.
- (10) Kinsinger, M. I.; Sun, B.; Abbott, N. L.; Lynn, D. M. Reversible Control of Ordering Transitions at Aqueous/Liquid Crystal Interfaces Using Functional Amphiphilic Polymers. *Adv. Mater.* **2007**, *19* (23), 4208–4212.
- (11) Price, A. D.; Schwartz, D. K. DNA Hybridization-Induced Reorientation of Liquid Crystal Anchoring at the Nematic Liquid Crystal/Aqueous Interface. *J. Am. Chem. Soc.* **2008**, *130* (26), 8188–8194.
- (12) Brake, J. M.; Abbott, N. L. Coupling of the Orientations of the Thermotropic Liquid Crystals to Protein Binding Events at Lipid-Decorated Interfaces. *Langmuir* **2007**, *23* (16), 8497–8507.
- (13) Brake, J. M.; Daschner, M. K.; Luk, Y. Y.; Abbott, N. L. Biomolecular Interactions at Phospholipid-Decorated Surfaces of Liquid Crystals. *Science* **2003**, *302* (5653), 2094–2097.
- (14) Hartono, D.; Bi, X.; Yang, K. L.; Yung, L. Y. L. An Air-Supported Liquid Crystal System for Real-Time and Label-Free Characterization of Phospholipases and Their Inhibitors. *Adv. Funct. Mater.* **2008**, *18* (19), 2938–2945.
- (15) Hu, Q.; Jang, C. H. Liquid Crystal-Based Imaging of Enzymatic Reactions at Aqueous-Liquid Crystal Interfaces Decorated with Oligopeptide Amphiphiles. *Bull. Korean Chem. Soc.* **2010**, *31* (5), 1262–1266.
- (16) Hussain, Z.; Zafiu, C.; Küpcü, S.; Pivetta, L.; Hollfelder, N.; Masutani, A.; Kilickiran, P.; Sinner, E. K. Liquid Crystal Based Sensors Monitoring Lipase Activity: A New Rapid and Sensitive Method for Cytotoxicity Assays. *Biosens. Bioelectron.* **2014**, *56*, 210–216.
- (17) Wang, Y.; Hu, Q.; Tian, T.; Gao, Y.; Yu, L. A Liquid Crystal-Based Sensor for the Simple and Sensitive Detection of Cellulase and Cysteine. *Colloids Surf., B* **2016**, *147*, 100–105.
- (18) Sun, H.; Yin, F.; Liu, X.; Jiang, T.; Ma, Y.; Gao, G.; Shi, J.; Hu, Q. Development of a Liquid Crystal-Based α -Glucosidase Assay to Detect Anti-Diabetic Drugs. *Microchem. J.* **2021**, *167*, 106323.
- (19) Lu, S.; Guo, Y.; Qi, L.; Hu, Q.; Yu, L. Highly Sensitive and Label-Free Detection of Catalase by a H₂O₂-Responsive Liquid Crystal Sensing Platform. *Sens. Actuators, B* **2021**, *344*, 130279.
- (20) Hu, Q. Z.; Jang, C. H. Using Liquid Crystals for the Real-Time Detection of Urease at Aqueous/Liquid Crystal Interfaces. *J. Mater. Sci.* **2012**, *47* (2), 969–975.
- (21) Tripathi, A.; Wolter, T. J.; Twieg, R. J.; Mavrikakis, M.; Abbott, N. L. Responsive Liquid Crystalline Materials Based on Interfacial Photocatalytic Processes. *Chem. Mater.* **2025**, *37* (9), 3221–3235.
- (22) Karaman, D.; Saylam, A.; Akar, E.; özçubukçu, S.; Bukusoglu, E. Liquid Crystals That Respond to the Aqueous Phase Reactions Catalyzed by Synthetic Enzyme Mimics. *Adv. Mater. Interfaces* **2025**, *12*, 1–13.
- (23) Dobson, C. M. Protein Folding and Misfolding. *Nature* **2003**, *426* (6968), 884–890.
- (24) Bilal, M.; Cui, J.; Iqbal, H. M. N. Tailoring Enzyme Microenvironment: State-of-the-Art Strategy to Fulfill the Quest for Efficient Bio-Catalysis. *Int. J. Biol. Macromol.* **2019**, *130*, 186–196.
- (25) Gulseren, G.; Khalily, M. A.; Tekinay, A. B.; Guler, M. O. Catalytic Supramolecular Self-Assembled Peptide Nanostructures for Ester Hydrolysis. *J. Mater. Chem. B* **2016**, *4* (26), 4605–4611.
- (26) Nothling, M. D.; Ganesan, A.; Condit-Jurkic, K.; Pressly, E.; Davalos, A.; Gotrik, M. R.; Xiao, Z.; Khoshdel, E.; Hawker, C. J.; O'Mara, M. L.; Coote, M. L.; Connal, L. A. Simple Design of an Enzyme-Inspired Supported Catalyst Based on a Catalytic Triad. *Chem* **2017**, *2* (5), 732–745.
- (27) Al-Garawi, Z. S.; McIntosh, B. A.; Neill-Hall, D.; Hatimy, A. A.; Sweet, S. M.; Bagley, M. C.; Serpell, L. C. The Amyloid Architecture Provides a Scaffold for Enzyme-like Catalysts. *Nanoscale* **2017**, *9* (30), 10773–10783.
- (28) Zaramella, D.; Scrimin, P.; Prins, L. J. Catalysis of Transesterification Reactions by a Self-Assembled Nanosystem. *Int. J. Mol. Sci.* **2013**, *14* (1), 2011–2021.
- (29) Liu, J.; Ohta, S. I.; Sonoda, A.; Yamada, M.; Yamamoto, M.; Nitta, N.; Murata, K.; Tabata, Y. Preparation of PEG-Conjugated Fullerene Containing Gd³⁺ Ions for Photodynamic Therapy. *J. Controlled Release* **2007**, *117* (1), 104–110.
- (30) Soyler, D.; Dolgun, V.; Kurbanoglu, S.; özçubukçu, S.; Soylemez, S. Synthesis and Design of Functional Fullerene-Based Electrochemical Nanobiosensor to Examine the Inhibition Effects of Anti-Alzheimer Drug Active Pyridostigmine on Acetylcholinesterase. *Measurement* **2025**, *253*, 117494.
- (31) Chaudhuri, P.; Paraskar, A.; Soni, S.; Mashelkar, R. A.; Sengupta, S. Fullerene-Cytotoxic Conjugates for Cancer Chemotherapy. *ACS Nano* **2009**, *3* (9), 2505–2514.
- (32) Sun, Y.; Cao, C.; Huang, P.; Yang, S.; Song, W. Amines Functionalized C₆₀ as Solid Base Catalysts for Knoevenagel Condensation with High Activity and Stability. *RSC Adv.* **2015**, *5* (105), 86082–86087.
- (33) Gülseren, G.; Saylam, A.; Marion, A.; özçubukçu, S. Fullerene-Based Mimics of Biocatalysts Show Remarkable Activity and Modularity. *ACS Appl. Mater. Interfaces* **2021**, *13* (38), 45854–45863.
- (34) Yeniterzi, D.; Demirsoy, Z.; Saylam, A.; özçubukçu, S.; Gülseren, G. Nanoarchitectonics of Fullerene-Based Enzyme Mimics for Osteogenic Induction of Stem Cells. *Macromol. Biosci.* **2022**, *22* (9), 1–11.
- (35) Soylemez, S.; Dolgun, V.; özçubukçu, S. Fullerene-Based Mimics of Enhanced Acetylcholine Detection for the Diagnosis of Alzheimer's Disease. *Microchem. J.* **2023**, *193*, 1–9.
- (36) Demirsoy, Z.; Gulseren, G. Self-Assembled Fullerene Nanostructures for Mimicking and Understanding of Natural Enzymes. *ACS Appl. Nano Mater.* **2022**, *5* (10), 14285–14295.
- (37) Loudet, J.-C.; Barois, P.; Poulin, P. Colloidal Ordering from Phase Separation in a Liquid-Crystalline Continuous Phase. *Nature* **2000**, *407* (6804), 611–613.
- (38) Hyun, C. K.; Choi, J. H.; Kim, J. H.; Ryu, D. D. Y. Enhancement Effect of Polyethylene Glycol on Enzymatic Synthesis of Cephalaxin. *Biotechnol. Bioeng.* **1993**, *41* (6), 654–658.
- (39) Pasut, G.; Sergi, M.; Veronese, F. M. Anti-Cancer PEG-Enzymes: 30 Years Old, but Still a Current Approach. *Adv. Drug Delivery Rev.* **2008**, *60* (1), 69–78.
- (40) Carlton, R. J.; Gupta, J. K.; Swift, C. L.; Abbott, N. L. Influence of Simple Electrolytes on the Orientational Ordering of Thermotropic Liquid Crystals at Aqueous Interfaces. *Langmuir* **2012**, *28* (1), 31–36.
- (41) Carlton, R. J.; Ma, C. D.; Gupta, J. K.; Abbott, N. L. Influence of Specific Anions on the Orientational Ordering of Thermotropic Liquid Crystals at Aqueous Interfaces. *Langmuir* **2012**, *28* (35), 12796–12805.